Delft University of Technology

Simulation of the Transition Phase for an Optimally-Controlled Tethered VTOL Rigid Aircraft for AirborneWind Energy Generation

Rushdi, Mostafa; Hussein , Ahmed A.; Dief, Tarek; Yoshida, Sheigeo; Schmehl, Roland

Important note
To cite this publication, please use the final published version (if applicable).
Please check the document version above.

Check for
updates

Simulation of the Transition Phase
for an Optimally-Controlled Tethered VTOL Rigid Aircraft
for Airborne Wind Energy Generation

Mostafa A. Rushdi*

Interdisciplinary Graduate School of Engineering Sciences, Kyushu University
6-1 Kasugakoen, Kasuga, Fukuoka 816-8580, Japan
Faculty of Engineering and Technology, Future University in Egypt (FUE),
5th Settlement, New Cairo 11835, Egypt

Ahmed A. Hussein[†]

Aerospace and Ocean Engineering, Viriginia Tech, 24061, USA

Tarek N. Dief[‡] and Sheigeo Yoshida[§]

Research Institute for Applied Mechanics, Kyushu University
6-1 Kasugakoen, Kasuga, Fukuoka 816-8580, Japan

Roland Schmehl[¶]

Delft University of Technology, Faculty of Aerospace Engineering
Kluyverweg 1, 2629HS, Delft, The Netherlands

Airborne wind energy (AWE) is an innovative renewable energy technology, with the potential to substantially reduce the cost of energy. This paper introduces a solution for one of the main challenges of AWE systems, which is the automated reliable launching of the airborne system component. Our launch system configuration consists of a rigid-wing flying object (aircraft) equipped with a VTOL subsystem and launched vertically, with the fuselage also directed vertically. We formulate the Transition phase as an optimal control problem, so as to determine the optimal control inputs which constitute the control surface deflections and the thrust force; which steers the aircraft from hovering with its nose upwards to forward flight. Subsequently, we simulate the trajectory for two cases of optimality; (a) minimizing the power consumption and (b) minimizing the endurance, during this phase. Choosing the case of minimizing power is more reasonable for our application, as the time interval difference between the two cases is almost 3 seconds only, but with a huge difference in the power consumed. We present a detailed mathematical analysis of the system followed by extensive simulation results.

I. Nomenclature

Latin Symbols

m	=	Aircraft mass
g	=	Magnitude of the gravitational acceleration (intensity of the gravitational field)
$\boldsymbol{I}$	=	Inertia matrix $\in R^{3\times3}$
S_w	=	Wing Area
b	=	Wing span
$\bar{c}$	=	Mean chord

*PhD Candidate, Kyushu University, rushdi.mostafa@riam.kyushu-u.ac.jp/ mostafa_rushdi@kyudai.jp /Mostafa.Roshdi@fue.edu.eg

[†]Postdoctoral researcher, Viriginia Tech, amonem@vt.edu

[‡]Postdoctoral researcher, Kyushu University, tarek.na3em@riam.kyushu-u.ac.jp

[§]Professor, Kyushu University, yoshidas@riam.kyushu-u.ac.jp

[¶]Associate Professor, Delft University of Technology, R.Schmehl@tudelft.nl

1

AR	=	Aspect ratio
V	=	aircraft speed
C_{i_j}	=	with $i = [X, Y, Z, l, m, n]$ and $j = [\alpha, \beta, p, q, r, \delta_a, \delta_e, \delta_r, 0]$ denote the dimensionless aerodynamic derivatives
F_T	=	Thrust force
$\boldsymbol{F}_a^B$	=	Aerodynamic force vector in the body frame; contains $[F_x, F_y, F_z]$
$\boldsymbol{M}_a^B$	=	Aerodynamic moment vector in the body frame; contains $[L, M, N]$
$\boldsymbol{u}$	=	Control action vector

Greek Symbols

α	=	Angle of attack
β	=	Side slip angle
ϕ	=	Roll angle
θ	=	Pitch angle
δ_e	=	Elevator deflection angle
$\boldsymbol{\omega}$	=	Angular velocity $\in R^{3\times1}$

Subscript and Superscript

a	=	Aerodynamic (when mentioned with vectors)
e	=	Elevator
r	=	Rudder
a	=	Aileron (when mentioned with δ)
f	=	Final
B	=	Body axis
$*$	=	Optimal

Abbreviations

AWE	=	Airborne Wind Energy
AP	=	Ampyx Power
$VTOL$	=	Vertical Take-off Landing
$ICLOCS$	=	Imperial College London Optimal Control Software
$IPOPT$	=	Interior-Point OPTimizer

II. Introduction

Airborne wind energy (AWE) is a class of innovative renewable energy technologies that employ by tethered flying devices for generating electricity [1–16]. In the following we refer to these devices as aircrafts. Because AWE systems do not require a heavy tower or foundations, substantial material savings can be achieved [1, 2]. In contrast to towered wind turbines, AWE systems are flying in the air, and mechanically connected to the ground (e.g., tethered kites or tethered balloons, which employ a tether for ground connection), which allows an exploitation of the relative velocity between the airmass of the AWE vehicle and the ground. The prominent reasons for the particular use of AWE in electricity production are (a) AWE systems reach winds blowing at higher-altitude atmospheric layers that are inaccessible by traditional wind turbines. These winds are typically stronger and more consistent than those closer to the ground, (b) the area that can be swept by an AWE system is not tightly limited, unlike that of a turbine which is limited by its diameter, and hence an AWE system is inherently more efficient, and (c) AWE systems are expected to need less material investment per unit of usable power than most other renewable energy sources. An important share of the worldwide primary energy could be potentially extracted from high-altitude winds. Two prominent AWE system architectures are Ground-Gen systems in which the conversion of mechanical energy into electrical energy takes place on the ground and Fly-Gen systems in which such conversion is done on the flying object or vehicle. A kite constituting

an AWE system is an ingeniously engineered airfoil having high-tech tethers that are fifteen times as strong as steel. A tether is a rope to tie something to a post or other fixed place, usually so that it can move freely within a relatively small area. Tether dynamics are extremely complex with numerous factors affecting the behavior of a cable – from the shape and aerodynamics of the tether to the elasticity, bending and torsion of the materials used, not to mention the changing wind speed and the low temperature at heights of up to 20 km. There are many scholarly papers exploring energy harvesting by tethered kites [17, 18]. However, very few established design guidelines for AWE systems currently exist [19].

It is clear that AWE systems are developing fast and are going to cover a great share in wind energy consumption. We could predict that this may happen within a few years from now, based on the rapid progress in AWE technology and on the continuous flow of research funds in the past few years [1]. Cherubini et al. [10] assert that the AWE research community is growing fast, indeed. They point out that this community is evenly divided between academia (where many of the best technical universities worldwide are involved), and industry (where decades-old companies face fierce competition by start-up ones). A detailed classification of emerging various AWE systems as well as listings of the most prominent universities and companies working contemporarily on the development of these systems are reported in [10]. A comparison of the patents and scientific papers produced in the AWE domain is given in [9]. Due to space limitations, we restrict our discussion of AWE systems herein to the paradigm of vertical take-off and landing (VTOL) [4, 6, 13–16].

A crucial challenge for AWE technology is how to automate the procedures of launching and landing for wing kite power systems, whether they are flexible or rigid. These procedures are required to be robust and reliable under various weather conditions. In the case of flexible wings or soft kites, this requirement is a big issue due to the proportional relation between the kite area and the power generated. There are some attempts to solve this problem by connecting the kite to a quadcopter which drags it to the operational altitude [4, 5]. This solution has many advantages, including the feasibility of launching in an arbitrary direction, that the setup time is satisfactorily short, and that no additional infrastructure is required. However, this solution is still partially ineffective with bigger kites, which have heavy non-uniformly distributed weights. This could be solved by using more than one quadcopter, but this leads to a complex swarm robotics problem, which must be solved to secure the connections among the quadcopters and that they will work together in unison serving the same goal [20]. In practice, several companies like Makani, E-kite, Twing Tec, kitemill [7, 8] and Skypull SA [6] go for the rigid wing design to simplify the process of vertical take-off and landing (VTOL). Several papers by Fagiano and his associates [6, 13–16] address important issues related to the VTOL paradigm. Of paramount importance is the issue of transitions experienced by the AWE vehicle from a hovering mode (where it acts as a multi-copter) to a dynamic-flight mode (where it acts like an airplane), and vice versa. For take-off and landing phases, the AWE vehicle uses multiple rotors to hover, while for the power generation phase, the vehicle exploits the aerodynamic forces generated by its wings to fly like a conventional plane. A crucial aspect from the point of view of control design is how to model and simulate the transition from one mode to the other.

The remainder of this paper is structured as follows. Section III overviews the full power cycle of the pertinent AWE aircraft and identifies this cycle to consist of three phases, namely: VTOL, transition, and flight mode. Out of these three phases, the transition phase is singled out for investigation, simulation, and control in this paper. Section IV constructs a mathematical model for the AWE aircraft under study by identifying the aerodynamic forces and moments affecting it, and writing down its kinetic equations using the typical formulation of optimal control problems. These equations are carefully verified for dimensional homogeneity [21]. Next, the equations are solved in Section V by a special piece of software that transforms the underlying optimal control problem into a static optimization problem. This section also reports and discusses the results obtained. Section VI concludes the paper.

III. Overview of the Full Power Cycle

The ultimate goal of our ongoing work is to simulate and control the dynamic model of a VTOL rigid aircraft connected to a tether to make a pumping cycle for power generation. However, in this paper, we confine our main focus to simulating and controlling the aircraft in the transition phase only. The aircraft simulation model represents the AP-2 aircraft, which has been developed by the Ampyx Power company [22–24]. The AP-2 aircraft was not initially designed for VTOL, but we want to see what happens if we modify it by adding vertical takeoff-landing capabilities. We assume that there are four propellers mounted to make the quadrotor conventional shape, so that the aircraft will behave as a tail-sitter aircraft, i.e., a VTOL aircraft that takes off and lands on its tail, then tilts horizontally for forward flight [25]. Also, we assume that the aircraft rotors or propellers are foldable. Relevant aircraft parameters are summarized in Table 1 and a visualization of the aircraft is shown in Fig. 1.

To give the reader a glimpse of the overall picture, we note that the operation of the full power cycle (Fig. 2) could

3

Fig. 1   A photograph of the AP-2 aircraft developed by Ampyx Power.

Table 1   Aircraft parameters

Parameter	Symbol	Value	Units
Aircraft mass	m	36.8	$[Kg]$
Inertia	$I_{x,y,z,xz}$	25, 32, 56, -0.47	$[Kg\ m^2]$
Wing Area	S_w	3	$[m^2]$
Wing span	b	5.5	$[m]$
Mean chord	$\bar{c}$	0.5	$[m]$
Aspect ratio	AR	10	$[-]$

be divided into 3 phases or stages:

1) **VTOL:** The aircraft takes advantage of the thrust of the four propellers to go up vertically. This phase is modeled by the equations of quadcopter (neglecting the drag contribution of the fuselage and the tether effect). The main challenge in this phase is that the aircraft fuselage is facing the crosswind, which makes a stability issue (the wind stream directly hits the horizontal tail which creates a moment that rotates the aircraft). Controlling the rotors must be fast to adjust any disturbance and sustain the aircraft on a vertical path.

2) **Transition:** The aircraft speeds up and rotates quickly enough to attain the altitude and reference speed that sustain its weight during the forthcoming flight mode. The main challenge in this phase is to capture the optimal operation point, which makes the transition path smooth enough, and which ensures that there is no losing of lift during the rotation. Also, the controller must respond in a fast way to give the exact deflections that result in a smooth path, after overcoming the disturbances from the crosswind. This phase of the full cycle could be formulated as a standard optimal control problem. We start such a formulation by deriving the state equations, which serve as the underlying constraints. The boundary conditions will be a hovering state as an initial state and a forward flight state as a final state. We follow this by writing the Hamiltonian formulation so as to derive the co-state equations. Choosing the suitable cost function is an important issue. For the current problem it could be to maximize the lift, i.e., to maximize the tension in the tether, which amounts to producing the maximum power during the transition path.

3) **Flight Mode:** The propellers are folded and the aircraft flies as a glider following the prescribed figure-of-eight path, according to the modular control strategy illustrated in [7, 8]. This strategy takes the form of a state machine as well as a cascaded flight control structure. The cascade flight control structure consists of:

   - **Guidance Module:** Based on the phase traction/retraction, this unit calculates the commanded course and the path angle beside their time rates of change,
   - **Path Loop:** This unit tracks the commands from the guidance module and calculates attitude commands

4

for the aerodynamic bank angle and the angle of attack,

- **Attitude Loop:** This unit tracks the attitude commands and transforms them into roll-, pitch-, and yaw rate commands,
- **Rate Loop:** This unit calculates the control moments which are then distributed among the actuators in the next unit,
- **Control Allocation Block:** This unit results in an aileron command, and
- **Winch Controller:** This is used to perform the retraction.

To have a simple overview, we could consider that the task of the flight control system is to control the tangential motion on a unit sphere while the radial direction is controlled by the winch.
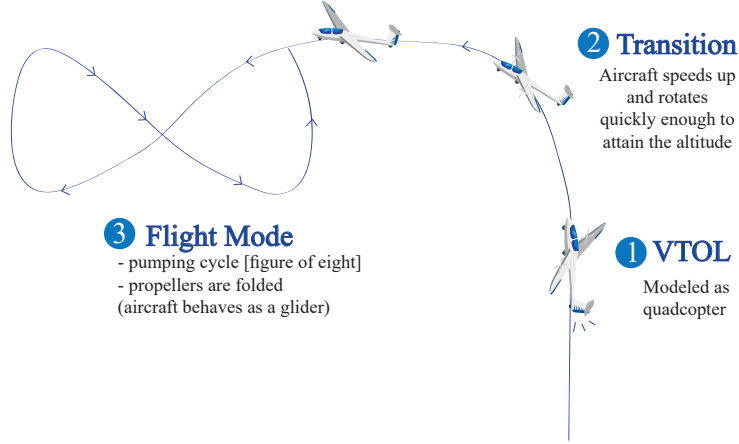

Fig. 2   Schematic summary of the phases of the full power cycle phases.

IV. Transition Phase

Normally a transition phase is difficult to be formulated and solved. There are some papers solving the transition phase from hovering to forward flight for several Unmanned Aerial Vehicles (UAVs) using several control techniques [25–29], and the back-way transition from forward flight to hovering for a tail-sitter UAV [29]. Also, for a flapping vehicle [30] there is a paper that simulates the transition phase using optimal control to minimize the time interval for this phase [31]. In this section, we give a mathematical model that hopefully captures the essence of the transition phase from hovering to forward flight. We model the longitudinal flight in the next subsection, then we represent the aerodynamic forces and moments. After that we introduce our optimal control formulation for this problem.

A. Mathematical Model

The mathematical model of a rigid-wing aircraft can be obtained using the six-degree-of-freedom Equations of Motion (EOM) that are used for modeling a conventional aircraft, i. e.,

$$m\dot{\boldsymbol{v}}^B = \boldsymbol{F}_a^B + \boldsymbol{F}_g^B - m(\boldsymbol{\omega}^B \times \boldsymbol{v}^B) \tag{1}$$

$$\boldsymbol{I}\dot{\boldsymbol{\omega}}^B = \boldsymbol{M}_a^B - (\boldsymbol{\omega}^B \times \boldsymbol{I}\boldsymbol{\omega}^B) \tag{2}$$

where the vector equation (1) represents the translational force and the vector equation (2) represents the angular momentum, both expressed in the body frame. The aircraft is subjected to an aerodynamic force $\boldsymbol{F}_a^B = [F_x, F_y, F_z]^T$, a gravity force $\boldsymbol{F}_g^B$ and an aerodynamic moment $\boldsymbol{M}_a^B = [L, M, N]^T$. Equations (1) and (2) in conjunction with equations for the rate of change of angular position and the rate of change of transnational position lead to the famous 12 equations for modeling a conventional aircraft. For steady conditions, we could decouple the longitudinal and lateral dynamics. We will focus on the longitudinal dynamics, which are represented by 4 equations, namely the rate of change of each of the axial velocity, the vertical velocity, the rotational velocity around the y-axis and the pitch angle.

$$\dot{u} = \frac{F_x}{m} - g \sin \theta + rv - qw \tag{3}$$

$$\dot{w} = \frac{F_z}{m} - g \sin \phi \cos \theta - ru + pw \tag{4}$$

$$\dot{q} = [M - (I_x - I_z)pr - I_{xz}(p^2 - r^2)]/I_y \tag{5}$$

$$\dot{\theta} = q \cos \phi - r \sin \phi \tag{6}$$

where F_x is the aerodynamic force in the x-direction in addition to the thrust force, g is the gravitational acceleration constant $\approx 9.81[m/s^2]$, $[u, v, w]$ are the velocity components in the x, y and z directions, respectively, $[p, q, r]$ are the angular velocities around the x, y and z axes, and $[\phi, \theta, \psi]$ are the roll, pitch and yaw angles, respectively. To assure full definition of the previous equations, we will present the aerodynamic model of this aircraft, which will define the aerodynamic forces and moments.

Aerodynamic forces and moments

The aerodynamic forces and moments are defined in the body frame as follow:

$$\boldsymbol{F}_a^B = \frac{1}{2} \rho V^2 S_w \begin{bmatrix} C_X \\ C_Y \\ C_Z \end{bmatrix} \tag{7}$$

$$\boldsymbol{M}_a^B = \frac{1}{2} \rho V^2 S_w \begin{bmatrix} b\, C_l \\ \bar{c}\, C_m \\ b\, C_n \end{bmatrix} \tag{8}$$

where $\rho \approx 1.225 kg/m^3$ is the air mass density, $V = \sqrt{u^2 + v^2 + w^2}$ is the aircraft speed, C_X, C_Y, C_Z and C_l, C_m, C_n are the non-dimensional body axes aerodynamic force and moment coefficients, respectively. It is common in the aerodynamic field to approximate the aerodynamic coefficients by linear terms in their series expansions [7, 8, 22–24]

$$C_X = C_{X_0} + C_{X_q} \left(\frac{\bar{c}q}{2V} \right) + C_{X_{\delta e}} \delta_e \tag{9}$$

$$C_Y = C_{Y_\beta} \beta + C_{Y_p} \left(\frac{bp}{2V} \right) + C_{Y_r} \left(\frac{br}{2V} \right) + C_{Y_{\delta a}} \delta_a + C_{Y_{\delta r}} \delta_r \tag{10}$$

$$C_Z = C_{Z_0} + C_{Z_q} \left(\frac{\bar{c}q}{2V} \right) + C_{Z_{\delta e}} \delta_e \tag{11}$$

$$C_l = C_{l_\beta} \beta + C_{l_p} \left(\frac{bp}{2V} \right) + C_{l_r} \left(\frac{br}{2V} \right) + C_{l_{\delta a}} \delta_a + C_{l_{\delta r}} \delta_r \tag{12}$$

$$C_m = C_{m_0} + C_{m_q} \left(\frac{\bar{c}q}{2V} \right) + C_{m_{\delta e}} \delta_e \tag{13}$$

$$C_n = C_{n_\beta} \beta + C_{n_p} \left(\frac{bp}{2V} \right) + C_{n_r} \left(\frac{br}{2V} \right) + C_{n_{\delta a}} \delta_a + C_{n_{\delta r}} \delta_r \tag{14}$$

We used a second-degree polynomial function to define the aerodynamic derivatives in terms of the angle of attack (α), i.e. $C(\alpha) = c_0 + c_1 \alpha + c_2 \alpha^2$. For example to fully define equation 9, we note that all the derivatives for AP-2 used below are available [22–24]

$$C_{X_0} = C_{X_{00}} + C_{X_{0_\alpha}} \cdot \alpha + C_{X_{0_{\alpha^2}}} \cdot \alpha^2$$
$$C_{X_q} = C_{X_{q0}} + C_{X_{q_\alpha}} \cdot \alpha + C_{X_{q_{\alpha^2}}} \cdot \alpha^2$$
$$C_{X_{\delta e}} = C_{X_{\delta e0}} + C_{X_{\delta e_\alpha}} \cdot \alpha + C_{X_{\delta e_{\alpha^2}}} \cdot \alpha^2$$

6

B. Optimal control problem formulation

The system of equations (3-6) could be written in abstract form as

$$\dot{x} = f(x, u) \tag{15}$$

where the state vector $x = [u, w, q, \theta]^T$ and $u = [\delta_e, F_T]$ represents the control actions, where F_T is the thrust force. The optimal control problem is to find a piecewise continuous control action $u(.) : [0, t_f^*] \rightarrow \Theta$ (admissible control set), that steers the system (15) from the hovering state to the forward flight state, using minimum energy. We chose the objective of our optimal control problem to be the minimization of energy consumption. Clearly this is because our target is to generate energy, so we have to minimize energy loss at each phase as much as possible, so that the net energy production will be higher. The cost function could be represented as follows:

$$\min_{u(.)} J = \int_0^{t_f^*} u^T u \, dt \tag{16}$$

Also, for the sake of comparison, we will also present results for the minimal-time problem, which is another minimization problem with a cost function represented as follows:

$$\min_{t_f} J = \int_0^{t_f^*} dt \tag{17}$$

We get the initial and final conditions by solving the nonlinear trim condition $\dot{x} = 0$. The initial state is defined as follows

$$x(t_0) = [u_0, w_0, q_0, \theta_0] = [0, 0, 0, \frac{\pi}{2}] \tag{18}$$

The aircraft, which is a tail-sitter, performs a hovering flight at this state, so there is no axial, vertical or rotational velocity. Also, the aircraft nose is upward, so the pitch angle is equal to 90°. There is still one remaining condition to sustain the aircraft at the hovering state without falling, which is that forces in the x direction should be equal (including thrust force) to the aircraft's weight.

The final state is defined as follow

$$x(t_f^*) = [u_f, w_f, q_f, \theta_f] = [15, 0, 0, 0] \tag{19}$$

At this state, the aircraft performs a normal forward flight, so there is some non-zero value for the axial velocity and the remaining parameters are each equal to zero. In the forward flight condition we are trying to find x such that the inertial forward speed is 15 m/s and $V_z = 0$.

The control action exerted by the elevator is bounded, due to the physical limitation

$$-30° < \delta_e < 30° \tag{20}$$

We don't have any limitation on the thrust force, except that our target is to find the minimum energy consumption. The thrust force will be a design parameter in modifying the AP-2 to perform VTOL. Also, we don't have any path constraints.

V. Solution and Results of the Optimal Control Problem

The optimal control problem defined in the previous section is then solved using the Imperial College London Optimal Control Software (**ICLOCS**) [32–34]. This is a MATLAB-based software, which allows users to define optimal control problems with general path and boundary constraints, and free or fixed final times [32]. The code also enables users to include constant design parameters as unknowns. As a prelude to its main function, the ICLOCS software transforms the given optimal control problem to a static optimization problem either by direct multiple shooting or by direct collocation methods [32]. The direct multiple shooting formulation requires the solution of initial value problems (IVPs) of ordinary differential equations (ODEs), while the direct collocation formulations discretize the system dynamics using implicit Runge-Kutta formulas [35, 36]. Once the optimal control problem has been transcribed as a static optimization problem, it can be solved with a prudent choice of nonlinear constrained optimization algorithms, e.g., by using the open source non-linear programming (NLP) solver called Interior-Point OPTimizer (**IPOPT**) [37–39] or

7

MATLAB's own NLP solver, namely its function **fmincon** [40, 41]. The derivatives of the underlying ODE right-hand side, cost and constraint functions are estimated numerically herein since they are required for the ICLOCS solution of the optimization problem. The discretized dynamical system of the optimal control problem is solved initially for an educated guess of the final time. The IPOPT solver continues to tackle the discretized problem until it reaches the minimum value of the consumed energy (16), or the minimum value of the final time (17), and then it terminates. The minimum consumed energy would correspond to the maximum net energy gained, while the minimum final time would represent the minimum/optimal time at which the transition between hovering and forward flight takes place.

Simulation results are presented in figures 3-10. Figures 3-6 represent the time history of the system states. Figures 7-8 represent the optimal control action variations with time. Finally, Fig. 10 represents the optimal path/trajectory. We solved our optimal control problem for the two cases denoted by the objective functions (16) and (17), namely:

- **Minimizing time**; with the cost function being represented by equation (17). In this case the flight endurance is minimized; $t_f^* = 2.7$ seconds.
- **Minimizing power**; with the cost function being represented by equation (16). In this case our target is to minimize the power expenditure, without any restriction on the flight endurance; $t_f = 5.825$ seconds.

The second case is more reasonable for our current application, as we are seeking the maximum net gain of power, i.e., we are striving to maximize the difference between wind-generated power and power consumption or expenditure by the flying vehicle during flight, which amounts to minimizing this power consumption.

Figure 3 shows the time history of the first state variable, which is the axial velocity u; the velocity in the direction of the aircraft's nose. In the beginning, while the vehicle is in the hovering mode and behaves as a multi-copter, the value of the axial velocity is zero and its direction is upward in the global axes. In the case of *minimizing time*; the aircraft's axial speed increases very fast, with a high slope and quickly exceeds the desired final axial velocity $u_f = 15 m/s$. Then it decreases until it saturates at u_f. In the case of *minimizing power*; the axial velocity increases to 6.4 m/sec in the first 1.1 seconds, then it decreases to zero at 3 seconds. After that, the axial velocity increases until it saturates directly at u_f, without any fluctuation around the final state.

Figure 4 shows the time history of the second state variable, which is the vertical velocity w. In the beginning, at the hovering state $w(0) = 0 m/s$, and at the final state $w(t_f) = 1.1 m/s$. In the case of *minimizing time*; the vertical velocity is almost zero for the beginning 0.34 seconds, then it starts to decrease until it reaches its peak at 2.106 seconds, the point of time that corresponds to the peak of the angular velocity q. After that, the vehicle is almost performing a forward flight and the vertical velocity w starts to increase until it saturates at the final state w_f. In the case of *minimizing power*; in the first 2.33 seconds the vertical velocity w fluctuates around zero. Then it starts to increase until almost 4.54 seconds, at which the aircraft begins to perform forward flight. After that, the vertical velocity w decreases and saturates at its final state.
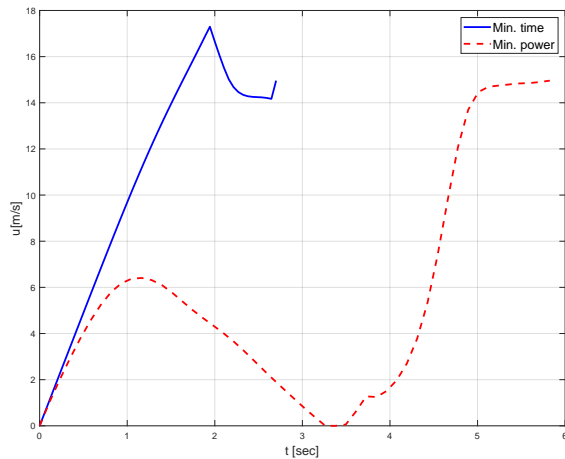

Fig. 3 Axial velocity u versus time, for our two distinct cases of optimization; minimizing time and minimizing power
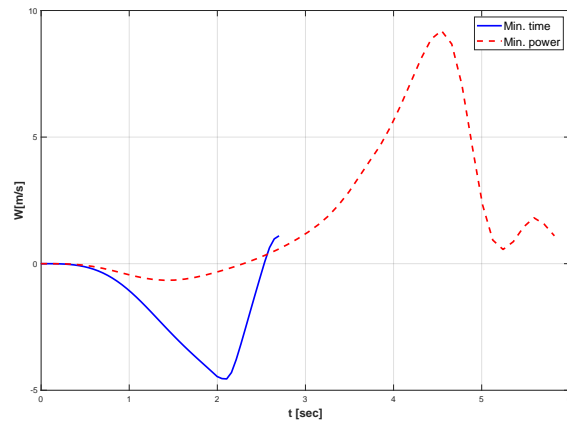

Fig. 4 Vertical velocity w versus time, for our two distinct cases of optimization; minimizing time and minimizing power
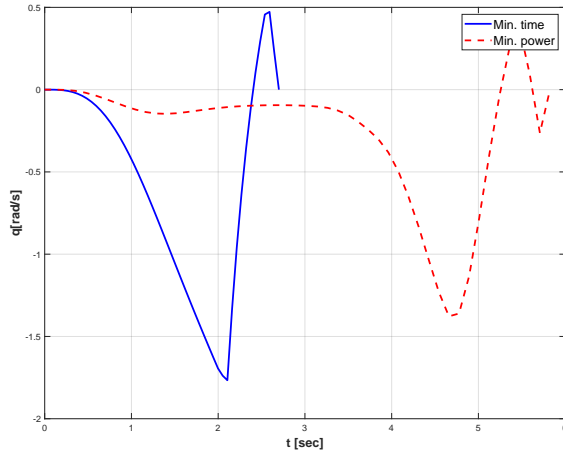
8

Fig. 5   Angular velocity q versus time, for our two distinct cases of optimization; minimizing time and minimizing power
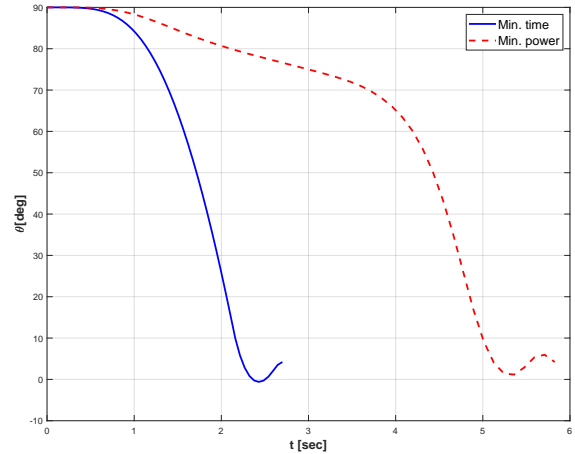

Fig. 6   Pitch angle θ versus time, for our two distinct cases of optimization; minimizing time and minimizing power

Figure 5 shows the time history of the third state variable, which is the angular velocity q. It starts with a zero value at the hovering state, then its value changes during the flight and returns to zero at the end. In the case of *minimizing time*; similarly to the vertical velocity, the angular velocity is almost zero for the beginning 0.34 seconds, then it starts to decrease until it reaches its minimum at 2.106 seconds, at which point the vehicle starts to perform forward flight, thereby acting as an aircraft. After that, the angular velocity starts to increase and returns to zero with some overshooting. In the case of *minimizing power*; in the first 3 seconds the angular velocity q is slightly below zero. Then it decreases until almost 4.66 seconds, within the region at which the aircraft starts to perform forward flight. After that, the angular velocity q increases and saturates at zero.

Figure 6 shows the time history of the fourth state variable, which is the pitch angle θ. The aircraft, which is a tail-sitter, is hovering at the beginning, so the pitch angle is equal to 90 degrees. Then the aircraft rotates until the trim conditions are reached at the final state. In the case of *minimizing time*; the aircraft almost remains at 90° in the first 0.59 seconds. Then the aircraft rotates in a fast way, as it turns from 90° to 10° in almost 1.55 seconds only. Finally, it makes a small fluctuation around its final state before it saturates. In the case of *minimizing power*; the aircraft almost remains at 90° in the first 0.815 seconds. Then it rotates gradually until reaching the final state with small fluctuation.

Figure 7 represents the non-dimensional thrust variation with time. In the case of *minimizing time*; this thrust is characterized by sudden, abrupt, and bang-bang changes. The non-dimensional thrust remains at the same value for 1.9 seconds, then it goes suddenly to zero for 0.6 seconds. In the case of *minimizing power*; the non-dimensional thrust makes some ups and downs until it saturates at almost zero at the final state; a reasonable behavior as the aircraft should start to behave as a glider.

Figure 8 represents the elevator deflection variation with time. In the case of *minimizing time*; similarly to the non-dimensional thrust, the elevator deflection follows a bang-bang fluctuation between two crisp bounds. The elevator deflection remains at 30° for the first 2 seconds, then it goes suddenly to −30° for 0.4 seconds. In the case of *minimizing power*; the elevator deflection fluctuates between −25° and 25° until 4.54 seconds, then it goes to −20° at the final state.

Figure 9 represents the non-dimensional power variation with time. In the case of *minimizing time*; the aircraft exerts a huge amount of power in the first 2 seconds, aiming to make the turning as fast as possible. On the other hand, in the case of *minimizing power*; the power values vary between 0 to 3, with most of the power exerted within the first 3 seconds. Note that the left vertical axis values are for the minimum time and the right vertical axis values are for the minimum power.

Figure 10 represents the optimal path/trajectory from hovering to forward flight. In the case of *minimizing time*; the aircraft spends around 7 meters hovering and rising up, then spends another 15 meters of height to turn. On the other side, in the case of *minimizing power*; the aircraft spends 12 meters hovering and rising up while rearranging its orientation. After that, the aircraft makes a forward flight without gaining any additional height.
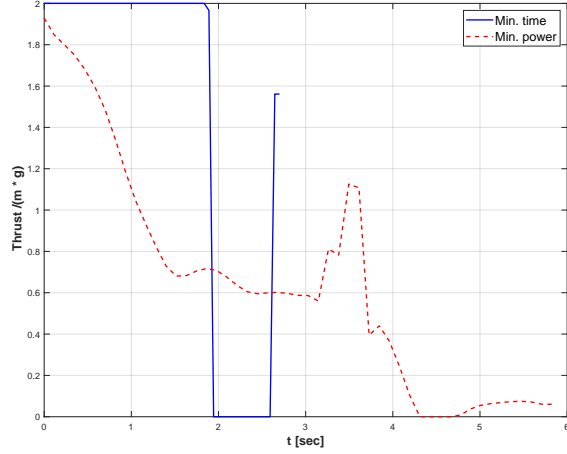
9

Fig. 7   Non-dimensional thrust versus time, for our two distinct cases of optimization; minimizing time and minimizing power
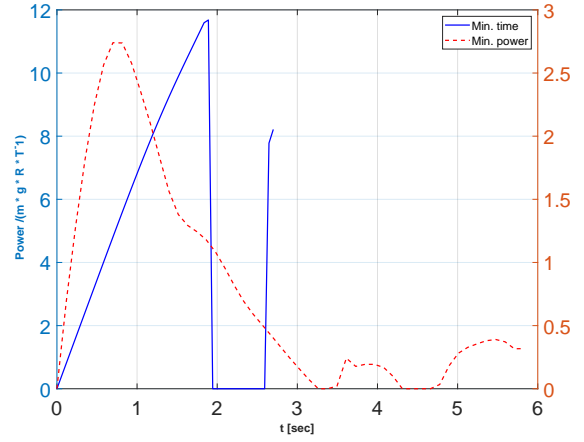

Fig. 9   Non-dimensional power versus time, for our two distinct cases of optimization; minimizing time and minimizing power
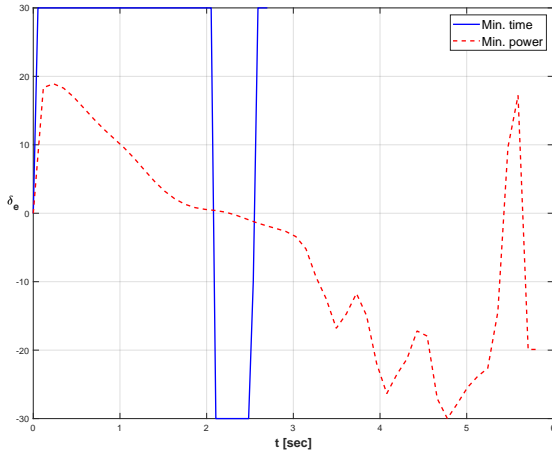

Fig. 8   Elevator deflection δ_e versus time, for our two distinct cases of optimization; minimizing time and minimizing power
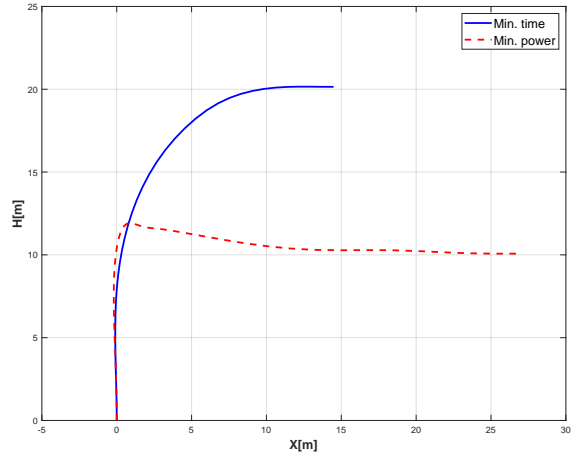

Fig. 10   Optimal trajectory/path from hovering to forward flight, represented by height (z axis) versus x axis, for our two distinct cases of optimization; minimizing time and minimizing power

VI. Conclusion

In this work we introduce a technique to find the optimal path in the transition phase, which is the middle phase among the three phases of the full power cycle for the studied AWE aircraft. Two optimality criteria are employed. Our genuine interest is to minimize the control action or the power consumption, or, equivalently, to maximize the net power gain. For comparison purposes, we also explored the possibility of minimizing the total time. Based on the aircraft characteristics, aerodynamic forces and moments, and boundary conditions of the pertinent optimal control problem, we made various simulations subject to each of the two optimality criteria. We could use each of the resulting two sets of simulations to achieve the desired optimal path. We calculated the required thrust over the transition phase, which is a design parameter needed for choosing the rotors capabilities. From the comparison, we found that time interval difference between the two cases is almost 3 seconds only, but with a huge difference in the power consumed. The minimization of energy in this phase will reduce the mass of the airborne component (battery) and this will have an effect on the harvesting and cut in wind speed. A forthcoming sequel of our current work is to extend our simulation so as to cover the full power cycle, including, in particular, simulation of the flight mode (figure of eight).

Acknowledgments

References

[1] Schmehl, R. (ed.), *Airborne wind energy: advances in technology development and research*, Green Energy and Technology, Springer, Singapore, 2018.

[2] Ahrens, U., Diehl, M., and Schmehl, R. (eds.), *Airborne Wind Energy*, Green Energy and Technology, Springer, Berlin Heidelberg, 2013.

[3] Rushdi, M., Yoshida, S., and Dief, T. N., "Simulation of a Tether of a Kite Power System Using a Lumped Mass Model," *IECES*, Fukuoka, Japan, 2018, pp. 42–47.

[4] Rapp, S., and Schmehl, R., "Vertical Takeoff and Landing of Flexible Wing Kite Power Systems," *Journal of Guidance, Control, and Dynamics*, Vol. 41, No. 11, 2018, pp. 2386–2400.

[5] Schanen, A., Dumon, J., Meslem, N., and Hably, A., "On Using Drones for the Take-off and Landing Phases of an AWE System," *Proceedings of the Airborne Wind Energy Conference*, 15-16 October 2019, p. 142.

[6] Todeschini, D., Fagiano, L., Micheli, C., and Cattano, A., "Control of vertical take off, dynamic flight and landing of hybrid drones for airborne wind energy systems," *2019 American Control Conference (ACC)*, IEEE, 2019, pp. 2177–2182.

[7] Rapp, S., Schmehl, R., Oland, E., Smidt, S., Haas, T., and Meyers, J., "A Modular Control Architecture for Airborne Wind Energy Systems," *AIAA Scitech 2019 Forum*, 2019, p. 1419.

[8] Rapp, S., Schmehl, R., Oland, E., and Haas, T., "Cascaded Pumping Cycle Control for Rigid Wing Airborne Wind Energy Systems," *Journal of Guidance, Control, and Dynamics*, 2019, pp. 1–18.

[9] Mendonça, A. K. d. S., Vaz, C. R., Lezana, Á. G. R., Anacleto, C. A., and Paladini, E. P., "Comparing patent and scientific literature in airborne wind energy," *Sustainability*, Vol. 9, No. 6, 2017, p. 915.

[10] Cherubini, A., Papini, A., Vertechy, R., and Fontana, M., "Airborne Wind Energy Systems: A review of the technologies," *Renewable and Sustainable Energy Reviews*, Vol. 51, 2015, pp. 1461–1476.

[11] Cherubini, A., Vertechy, R., and Fontana, M., "Simplified model of offshore airborne wind energy converters," *Renewable Energy*, Vol. 88, 2016, pp. 465–473.

[12] Samson, J., Katebi, R., and Vermillion, C., "A critical assessment of airborne wind energy systems," *2nd IET Renewable Power Generation Conference*, IET, 2013, pp. 4–7.

[13] Martin, P., Devasia, S., and Paden, B., "A different look at output tracking: control of a VTOL aircraft," *Automatica*, Vol. 32, No. 1, 1996, pp. 101–107.

[14] Fagiano, L., Nguyen-Van, E., Rager, F., Schnez, S., and Ohler, C., "Autonomous takeoff and flight of a tethered aircraft for airborne wind energy," *IEEE Transactions on Control Systems Technology*, Vol. 26, No. 1, 2017, pp. 151–166.

[15] Fagiano, L., Van, E. N., and Schnez, S., "Linear take-off and landing of a rigid aircraft for airborne wind energy extraction," *Airborne Wind Energy*, Springer, 2018, pp. 491–514.

[16] Fagiano, L., Nguyen-Van, E., Rager, F., Schnez, S., and Ohler, C., "Automatic Take-Off of a Tethered Aircraft for Airborne Wind Energy: Control Design and Experimental Results," *IFAC-PapersOnLine*, Vol. 50, No. 1, 2017, pp. 11932–11937.

[17] Loyd, M. L., "Crosswind kite power (for large-scale wind power production)," *Journal of energy*, Vol. 4, No. 3, 1980, pp. 106–111.

[18] Williams, P., Lansdorp, B., and Ockesl, W., "Optimal crosswind towing and power generation with tethered kites," *Journal of guidance, control, and dynamics*, Vol. 31, No. 1, 2008, pp. 81–93.

11

[19] Fagiano, L., and Marks, T., "Design of a small-scale prototype for research in airborne wind energy," *IEEE/ASME Transactions on Mechatronics*, Vol. 20, No. 1, 2014, pp. 166–177.

[20] Amin, S. M., Ibrahim, K. H., Al-Naggar, A., Nabil, A., El-Sadek, A., Abdel-Galil, M., and Badawi, A. H., "Parametrized Experience Exchange in Expert-Fellow Swarm Robotic System, Controller Performance Context," *AIAA Information Systems-AIAA Infotech@ Aerospace*, 2017, p. 1066.

[21] Rushdi, M. A., and Rushdi, A. M., "On the Fundamental Masses Derivable by Dimensional Analysis." *Journal of King Abdulaziz University: Engineering Sciences*, Vol. 27, No. 1, 2016, pp. 35–42.

[22] Licitra, G., "Identification and Optimization of an Airborne Wind Energy System," Ph.D. thesis, Albert Ludwig Univ. of Freiburg, Freiburg im Breisgau, Germany, 2018.

[23] Licitra, G., Bürger, A., Williams, P., Ruiterkamp, R., and Diehl, M., "System Identification of a Rigid Wing Airborne Wind Energy System," *arXiv preprint arXiv:1711.10010*, 2017.

[24] Licitra, G., Koenemann, J., Bürger, A., Williams, P., Ruiterkamp, R., and Diehl, M., "Performance assessment of a rigid wing Airborne Wind Energy pumping system," *Energy*, Vol. 173, 2019, pp. 569–585.

[25] Li, Z., Zhang, L., Liu, H., Zuo, Z., and Liu, C., "Nonlinear robust control of tail-sitter aircrafts in flight mode transitions," *Aerospace Science and Technology*, Vol. 81, 2018, pp. 348–361.

[26] Liu, Z., Guo, J., Li, M., Tang, S., and Wang, X., "VTOL UAV Transition Maneuver Using Incremental Nonlinear Dynamic Inversion," *International Journal of Aerospace Engineering*, Vol. 2018, 2018.

[27] Casau, P., Cabecinhas, D., and Silvestre, C., "Autonomous transition flight for a vertical take-off and landing aircraft," *2011 50th IEEE Conference on Decision and Control and European Control Conference*, IEEE, 2011, pp. 3974–3979.

[28] Zhou, J., Lyu, X., Li, Z., Shen, S., and Zhang, F., "A unified control method for quadrotor tail-sitter uavs in all flight modes: Hover, transition, and level flight," *2017 IEEE/RSJ International Conference on Intelligent Robots and Systems (IROS)*, IEEE, 2017, pp. 4835–4841.

[29] Kokume, M., and Uchiyama, K., "Control architecture for transition from level flight to hover of a fixed-wing UAV," *IECON 2011-37th Annual Conference of the IEEE Industrial Electronics Society*, IEEE, 2011, pp. 522–527.

[30] Elsadek, A., Taha, H. E., and El-Bayoumi, G. M., "Stability analysis of longitudinal dynamics of hovering flapping mavs/insects," *AIAA Atmospheric Flight Mechanics Conference*, 2017, p. 1635.

[31] Hussein, A. A., Seleit, A. E., Taha, H. E., and Hajj, M. R., "Optimal transition of flapping wing micro-air vehicles from hovering to forward flight," *Aerospace Science and Technology*, Vol. 90, 2019, pp. 246–263.

[32] Falugi, P., Kerrigan, E., and Van Wyk, E., "Imperial college london optimal control software user guide (ICLOCS)," *Department of Electrical and Electronic Engineering, Imperial College London, London, England, UK*, 2010.

[33] Nie, Y., Faqir, O., and Kerrigan, E. C., "ICLOCS2: Try this Optimal Control Problem Solver Before you Try the Rest," *2018 UKACC 12th International Conference on Control (CONTROL)*, IEEE, 2018, pp. 336–336.

[34] Foroozandeh, Z., do rosário de Pinho, M., and Shamsi, M., "On numerical methods for singular optimal control problems: An application to an AUV problem," *Discrete & Continuous Dynamical Systems-B*, Vol. 24, No. 5, 2019, p. 2219.

[35] Butcher, J. C., "Implicit runge-kutta processes," *Mathematics of Computation*, Vol. 18, No. 85, 1964, pp. 50–64.

[36] Fatunla, S. O., *Numerical methods for initial value problems in ordinary differential equations*, Academic Press, 2014.

[37] Biegler, L. T., and Zavala, V. M., "Large-scale nonlinear programming using IPOPT: An integrating framework for enterprise-wide dynamic optimization," *Computers & Chemical Engineering*, Vol. 33, No. 3, 2009, pp. 575–582.

[38] Wächter, A., "Short tutorial: getting started with ipopt in 90 minutes," *Dagstuhl Seminar Proceedings*, Schloss Dagstuhl-Leibniz-Zentrum für Informatik, 2009.

[39] Biegler, L. T., "Efficient nonlinear programming algorithms for chemical process control and operations," *IFIP Conference on System Modeling and Optimization*, Springer, 2007, pp. 21–35.

[40] Chuan, W., Lei, Y., and Jianguo, Z., "Study on optimization of radiological worker allocation problem based on nonlinear programming function-fmincon," *2014 IEEE International Conference on Mechatronics and Automation*, IEEE, 2014, pp. 1073–1078.

[41] Benhamida, F., "A New Solution Method to Economic Dispatch using the MATLAB Function (fmincon)," *Conference International AMSE MS*, Vol. 5, 2016.